Biomol NMR Assign (2015) 9:7–14
DOI 10.1007/s12104-013-9535-x

ARTICLE

Solid-state NMR sequential assignment of Osaka-mutant amyloid-beta (Aβ1−40 E22Δ) fibrils

Matthias Huber · Oxana Yu. Ovchinnikova · Anne K. Schütz · Rudi Glockshuber · Beat H. Meier · Anja Böckmann

Received: 16 August 2013 / Accepted: 12 December 2013 / Published online: 7 January 2014

Abstract Alzheimer's disease (AD) is the most common form of dementia. Aggregation of amyloid β (Aβ), a peptide of 39−43 residues length, into insoluble fibrils is considered to initiate the disease. Determination of the molecular structure of Aβ fibrils is technically challenging and is a significant goal in AD research that may lead to design of effective therapeutical inhibitors of Aβ aggregation. Here, we present chemical-shift assignments for fibrils formed by highly pure recombinant Aβ1−40 with the Osaka E22Δ mutation that is found in familial AD. We show that that all regions of the peptide are rigid, including the N-terminal part often believed to be flexible in Aβ wt.

Keywords Alzheimer's disease · Solid-state NMR spectroscopy · Amyloid beta · Amyloid structures · Fibrils

Matthias Huber and Oxana Yu. Ovchinnikova have contributed equally to this work.

M. Huber · A. K. Schütz · B. H. Meier (✉)
Laboratory of Physical Chemistry, ETH Zurich, Wolfgang Pauli Strasse 10, 8093 Zurich, Switzerland
e-mail: beme@ethz.ch

O. Y. Ovchinnikova · R. Glockshuber (✉)
Institute of Molecular Biology and Biophysics, ETH Zurich, Schafmattstrasse 20, 8093 Zurich, Switzerland
e-mail: rudi@mol.biol.ethz.ch

A. Böckmann (✉)
Institut de Biologie et Chimie des Protéines, UMR 5086 CNRS/Université de Lyon 1, 7 passage du Vercors, 69367 Lyon, France
e-mail: a.bockmann@ibcp.fr

Biological context

The aggregation of amyloid-β (Aβ, a peptide of 39−43 residues length) and accumulation in extracellular deposits in the brain are key events in Alzheimer's disease (AD), the most prevalent neurodegenerative disease in elderly people (Hardy and Selkoe 2002). Aβ is formed from proteolytic cleavage of the amyloid precursor protein (APP) by β- and γ-secretase. Aβ1−40 and Aβ1−42 are the main isoforms occurring in the human brain. Aβ1−42 is significantly less abundant than Aβ1−40 (Tomiyama et al. 2008) but is believed to have a higher tendency to aggregate (Irie et al. 2005). AD mostly occurs spontaneously with late onset. A small number of AD cases have a familial background, though, and are caused by mutations in the genes coding for APP or presenilin (Levy-Lahad et al. 1995). Recently, the Osaka mutation E22Δ within the Aβ sequence was found in Japanese AD patients (Tomiyama et al. 2008). Aβ1−40 E22Δ forms fibrils with a different EM signature than Aβ1−40 wt. It has an increased tendency to form fibrillar bundles, a higher thioflavin T binding capacity and is significantly more toxic in rat primary neurons than Aβ1−40 wt (Ovchinnikova et al. 2011), which might explain the early onset of AD caused by this mutation.

While Aβ is generally known to form amyloid fibrils, determination of its atomic-level structure has long been hampered since the classical tools, X-ray crystallography and solution NMR spectroscopy, cannot provide sufficient information. Solid-state NMR has recently become a method that provides atomic-level insights into the structure of insoluble and non-crystalline proteins (Debelouchina et al. 2010; Zech et al. 2005; Van Melckebeke et al. 2010; Castellani et al. 2003; Wasmer et al. 2008; Loquet et al. 2008; Manolikas et al. 2008; Franks et al. 2008).

Table 1 Experimental parameters for the NMR spectra

Experiment	NCACB	CANCoCX	NCOCX	CCC	NCACO	NcoCACB	NCA	DARR 15 ms
^{1}H Larmor frequency (MHz)	600	850	600	600	600	600	850	850
Isotope Labeling	[U−^{13}C^{15}N]	[U−^{13}C^{15}N]	[U−^{13}C^{15}N]	[U−^{13}C^{15}N]	[U−^{13}C^{15}N]	[U−^{13}C^{15}N]	[U−^{13}C^{15}N]	[U−^{13}C]
MAS frequency (kHz)	13	19	13	13	13	13	19	19
Transfer 1	HN-CP	HC-CP	HN-CP	HC-CP	HN-CP	HN-CP	HN-CP	HC-CP
Field (kHz)—^{1}H	71.1	72.8	81.6	130.4	70.7	74.1	62.3	75.8
Field (kHz)—X	59.0	61.6	54.4	119.6	57.6	46.8	62.5	63.0
Shape	Tangent	Tangent	Tangent	Tangent	Tangent	Tangent	Tangent	Tangent
Carrier (ppm)	–	CA	–	–	–	–	–	100
Time (ms)	1	0.4	1.2	0.5	1	1	1.2	1
Transfer 2	NC-CP	CN-CP	NC-CP	DREAM	NC-CP	NC-CP	NC-CP	DARR
Field (kHz)—^{1}H	94.4	93.3	109.7	97.7	79.4	83.1	88.1	18.7
Field (kHz)—^{13}C	4.1	6.2	4.3	15.7	4.3	3.9	10.8	–
Field (kHz)—^{15}N	17.7	13.0	16.7	–	18.6	16.6	24.0	–
Shape	Tangent	Tangent	Tangent	Tangent	Tangent	Tangent	Tangent	–
Carrier (ppm)	CA	CA	CO	55	CA	CO	CA	–
Time (ms)	6	5.5	4	4	5.5	7	6	15
Transfer 3	DREAM	NC-CP	DARR	DARR	DARR	MIRROR	–	–
Field (kHz)—^{1}H	94.4	83.1	12.9	12.8	13.4	17.9	–	–
Field (kHz)—^{13}C	6.0	6.2	–	–	–	–	–	–
Field (kHz)−^{15}N	–	13.4	–	–	–	–	–	–
Shape	Tangent	Tangent	–	–	–	–	–	–
Carrier (ppm)	59	CO	–	–	–	–	–	–
Time (ms)	3	5.5	50	50	10	10	–	–
Transfer 4	–	MIRROR	–	–	–	DREAM	–	–
Field (kHz)−^{1}H	–	15.9	–	–	–	91.2	–	–
Field (kHz)−^{13}C	–	–	–	–	–	6.0	–	–
Shape	–	–	–	–	–	Tangent	–	–
Carrier (ppm)	–	–	–	–	–	59	–	–
Time (ms)	–	30	–	–	–	3	–	–
t_1 increments	36	128	54	172	52	48	1,024	2,560
Sweep width (t_1) (kHz)	3.35	11.7	4	20	3.65	4	40	100
Max. acq time (t_1) (ms)	5.3	5.4	6.8	5.4	7.1	6	12.8	12.80
t_2 increments	90	64	96	172	108	100	1,280	3,072
Sweep width (t_1) (kHz)	8.3	4.3	6.8	20	8.3	9	83.3	100
Max. acq time (t_2) (ms)	5.4	7.3	7.1	5.4	6.5	5.5	15.4	15.36
t_3 increments	1,280	1,536	1,280	1,280	1,280	1,280	–	–
Sweep width (t_3) (kHz)	50	100	50	50	50	100	–	–
Max. acq time (t_3) (ms)	12.9	7.8	12.9	12.9	12.8	12.8	–	–
^{1}H Spinal-64Dec. (kHz)	90	88	91	91	85	86	91	100
Interscan delay (s)	1.8	2.6	2	1.9	1.4	1.6	2	2.5
Number of scans	8	16	16	4	32	32	8	2
Measurem. time (h)	13.1	95.5	47.7	64.6	71.4	69.6	4.6	3.6

Although numerous solid-state NMR studies on a multitude of polymorphs of Aβ fibrils have been published to date (reviewed in Tycko 2006, 2011; Bertini et al. 2011; Lopez del Amo et al. 2012) no atomic resolution structure has been obtained so far. A limiting step in the determination of the atomic-resolution structure of Aβ fibrils by solid-state NMR is the preparation of isotopically labeled Aβ fibrils in sufficient quantity, and, even more critical, in

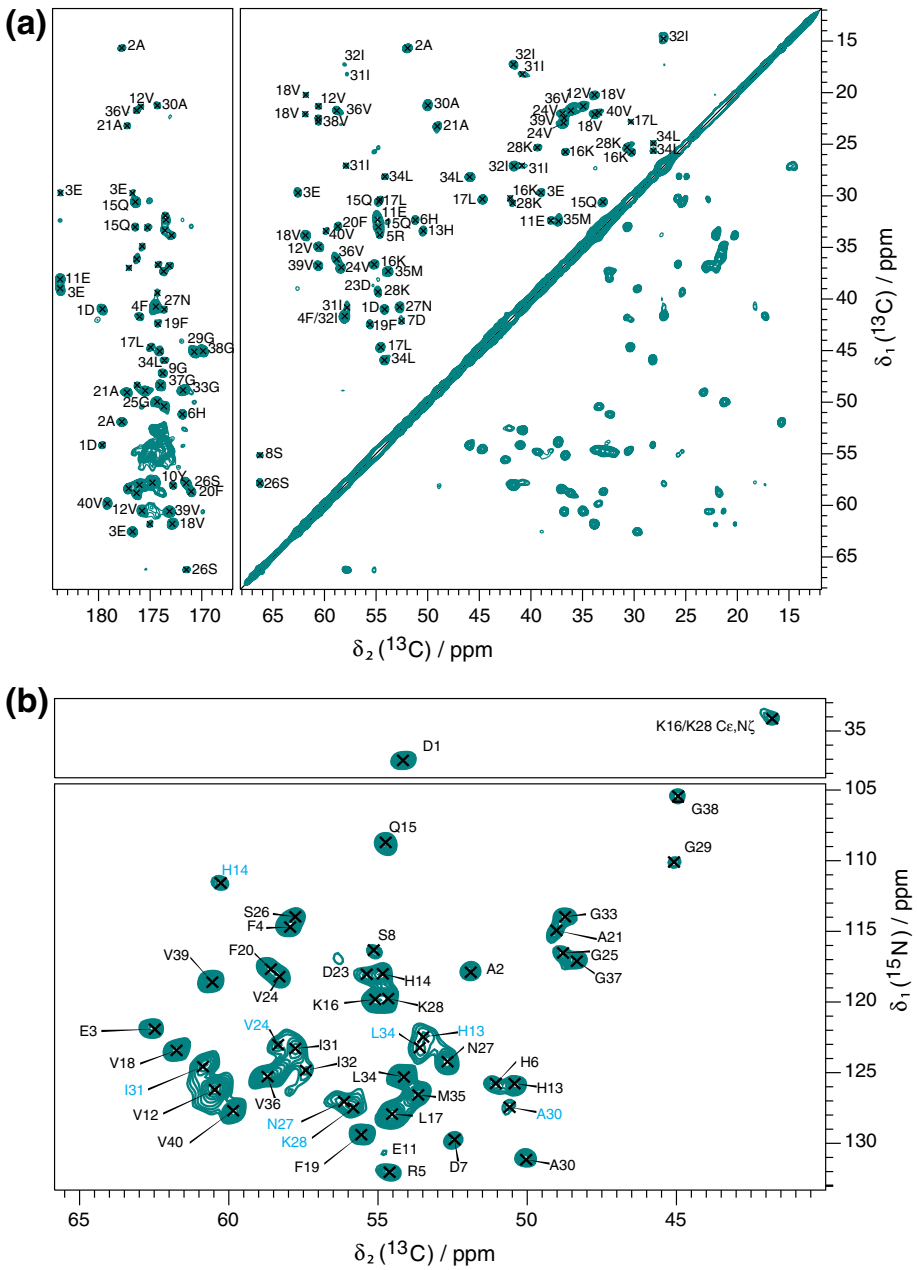

Fig. 1 Solid-state NMR spectra of Aβ1−40 E22Δ fibrils acquired at a magnetic field of 20.0 T and MAS at a frequency of 19 kHz. **a** 2D $^{13}C-^{13}C$ DARR spectrum with a mixing time of 15 ms measured on [$U-^{13}C$] labeled fibrils. **b** NCA spectrum of [$U-^{13}C,^{15}N$] labeled fibrils. The sequence specific assignments indicated were derived from a sequential backbone walk in 3D spectra as shown in Fig. 2. *Blue labels* correspond to peaks from a second minor polymorph with a much lower relative abundancea in the [$U-^{13}C$] sample

sufficient quality and conformational homogeneity to record high-resolution spectra. Only then, sequential resonance assignments can be achieved as a first step in 3D structure determination.

Methods and experiments

Preparation of [U−$^{13}C,^{15}N$]-Aβ1−40 E22Δ fibrils

The plasmid for expression in *Escherichia coli* of Aβ1−40 E22Δ has been described previously (Ovchinnikova et al. 2011). The expression was performed in *E. coli* BL21 (DE3) under T7 promoter control in M9 minimal medium containing 100 μM $CaCl_2$, 1 μM $FeCl_3$, 10 μM $ZnCl_2$, 1 mM $MgSO_4$, ^{13}C-glucose (2 g/L) and ^{15}N-NH_4Cl (1 g/L), and cells were induced at $OD_{600} \sim 1.0$ for 10 h at 37 °C with 1 mM IPTG. Aβ1−40 E22Δ was produced as a fusion to the peptide sequence $(NANP)_{19}$ with N-terminal hexahistidine tag and subsequently cleaved of the fusion protein with TEV protease as described earlier (Ovchinnikova et al. 2011). The high purity and identity of the peptide was verified by MALDI-TOF mass spectrometry using sinapinic acid as matrix (data not shown). Aβ1−40 E22Δ was dissolved in 10 mM NaOH to concentration of 150−200 μM and subjected to ultracentrifugation for 1 h at 135,500*g* and 4 °C. The stock solution was kept on ice and used for preparation of the fibrils within 24 h. The

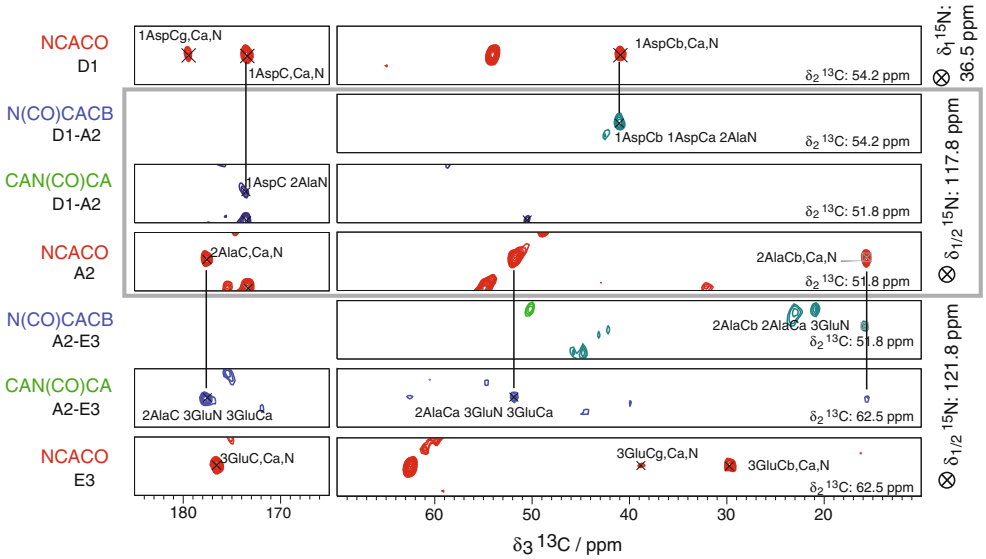

Fig. 2 Strips extracted from the 3D NCACO, N(CO)CACB and CAN(CO)CA spectra of fibrillar Aβ1−40 E22Δ. *Vertical lines* were added to aid following the backbone walk starting at the N-terminus of the protein

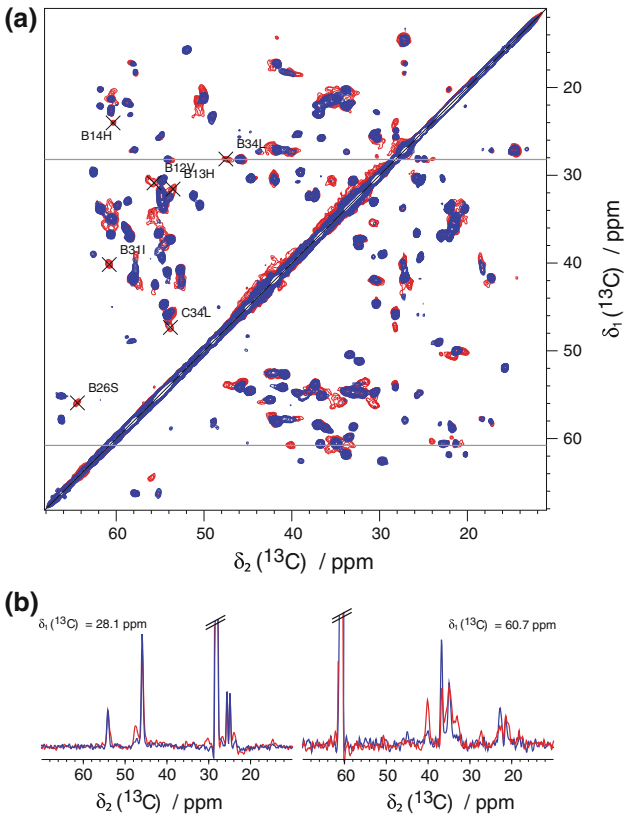

Fig. 3 **a** Overlay of 2D [^{13}C;^{13}C] DARR spectra (15 ms mixing, 19 kHz MAS, 20 T B_0) of Aβ1−40 E22Δ fibrils of two independent preparations of the sample. *Red* sample 1, [U−^{13}C, ^{15}N]. *Blue* sample 2, [U-^{13}C]. Polymorphic signals that are only observed in the sample 1 are labeled. The *letters B* and *C* in front of the residue names indicate polymorph B and C. Traces where 1D spectra were extracted are indicated by the *gray lines* at $\delta_1(^{13}C) = 28.1$ ppm and $\delta_1(^{13}C) = 60.7$ ppm **b** Traces from DARR spectra of Aβ1−40 E22Δ fibrils for the two independent preparations of the sample

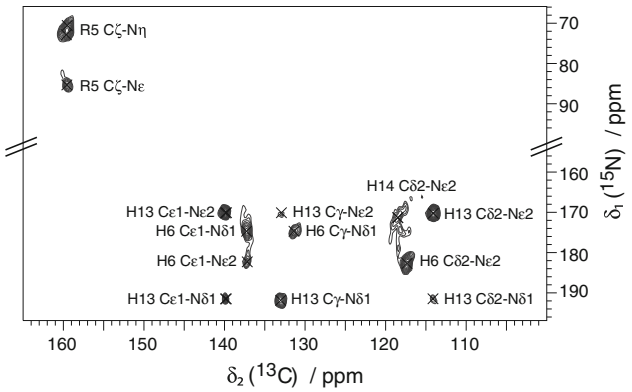

Fig. 4 [^{15}N;^{13}C] side-chain correlations of arginine and histidine side chains in a PAIN spectrum

aggregation reaction was performed at 37 °C and 700 revolutions per minute (rpm) with 35−50 μM Aβ (final concentration) in 10 mM H_3PO_4−NaOH pH 7.4 and 100 mM NaCl. The aggregation reaction was started by dilution of the Aβ stock solution in 10 mM NaOH with an aggregation buffer mix resulting in pH 7.4 and the final concentrations indicated above.

Sample preparation for NMR

The fibrils were centrifuged for 45 min at 29,400*g* and 4 °C, washed with MilliQ water and centrifuged again as described. The pellet containing approximately 12 mg Aβ1−40 E22Δ fibrils was resuspended in ca 400 μL MilliQ water and packed into a 3.2 mm ZrO_2 rotor (Bruker Biospin) using ultracentrifugation and a home made filling device (Böckmann et al. 2009), in a SW41-TI swing-out rotor spinning at 25,000 rpm

for 16 h in an optima L90-K ultracentrifuge (Beckmann). The drive tip of the rotor was sealed with epoxy glue (Araldit) to prevent dehydration of the sample.

NMR spectroscopy

We used two sets of 3D experiments for backbone assignments, namely NCOCA, NCACO and CANCO as well as NCACB, N(CO)CACB and CAN(CO)CA as described previously (Schuetz et al. 2010) and completed the side-chain assignment with 3D CCC and 2D DARR spectra. Spectra were recorded on a Bruker Advance II + spectrometer operating at 850 MHz ^{1}H Larmor frequency with magic-angle-spinning (MAS) at 19 kHz or on a Bruker Advance spectrometer operating at 600 MHz ^{1}H Larmor frequency at MAS frequency of 13 kHz. Spectra were processed with Topspin (Bruker Biospin) and analyzed with CCPN (Vranken et al. 2005; Stevens et al. 2011). Detailed experimental conditions are given in Table 1.

Chemical-shift analysis

Secondary chemical shifts were obtained by subtracting the random-coil shifts as tabulated in Wang and Jardetzky (2002) from the observed chemical shifts. Secondary structure was predicted using TALOS+ (Shen et al. 2009).

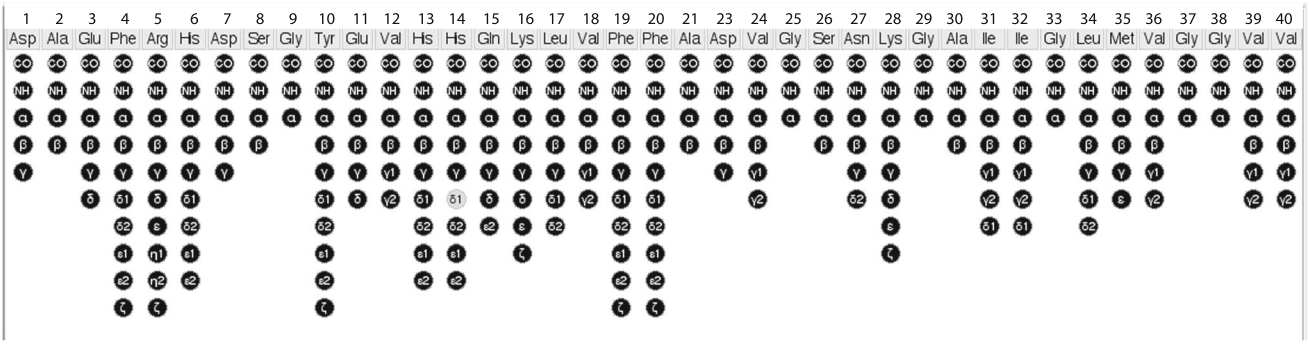

Fig. 5 Assignment graph of Aβ1−40 E22Δ created using the CCPN software (Stevens et al. 2011). *Black dots* indicate assigned spins, while the unassigned one is shown in *white*

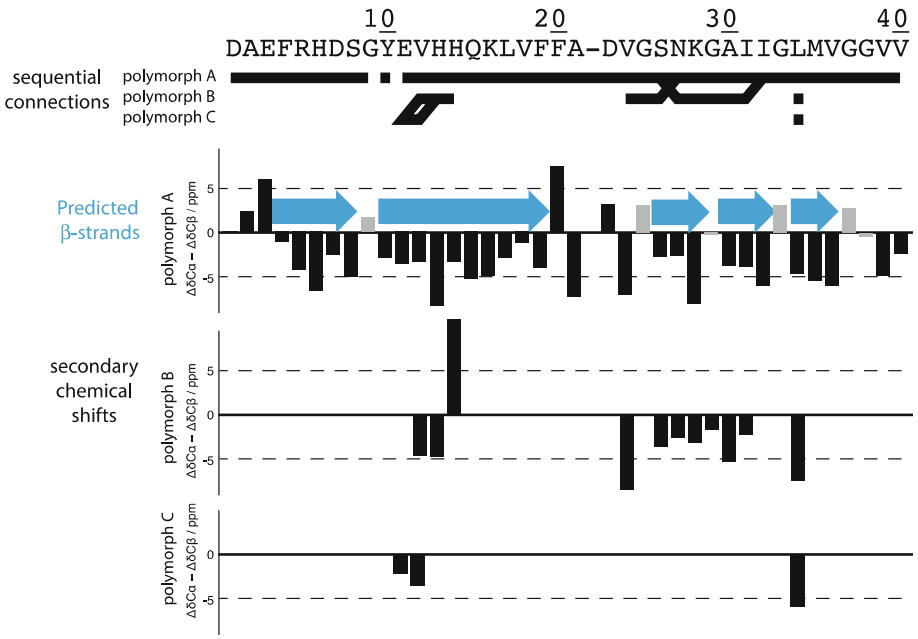

Fig. 6 Difference of Cα and Cβ secondary chemical shifts (Wishart and Sykes 1994) derived from sequential assignments in 3D spectra of labeled Aβ1−40 E22Δ fibrils. For glycine $\Delta\delta C_{\alpha}$ is plotted and the corresponding residues *bars* are plotted in *gray*. Three negative secondary shifts in a row are indicative for β-sheet structure. *Blue arrows* are drawn for TALOS+ predicted β-sheet regions where glycines were left out. The intensity of signal from polymorphs B and C varies for the different samples and is largest for the [$U-^{13}$C, ^{15}N] rotor (approx. 60 % that of polymorph A) and lowest in the [$U-^{13}$C] rotor (approx. 10 % of the intensity of polymorph A)

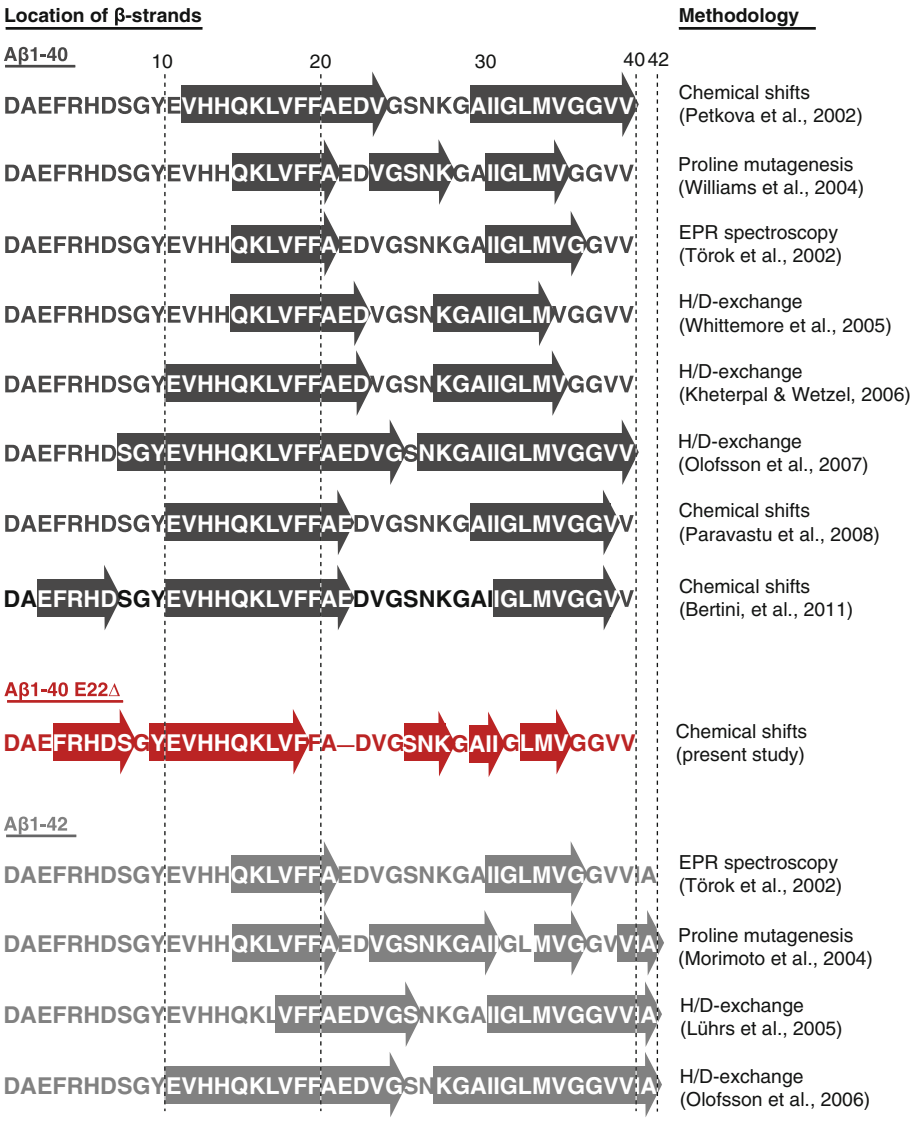

Fig. 7 Comparison of the secondary structure derived from the Aβ1−40 E22Δ sequential assignments presented here with values reported in the literature for Aβ1−40 and Aβ1−42

Only values without warning were considered and glycine residues were generally left out.

Assignment and data deposition

Fibrils of Aβ1−40 E22Δ yield 2D $^{13}C-^{13}C$ and $^{15}N-^{13}C$ spectra with narrow lines (linewidth typically 0.5 ppm) reflecting a homogenous sample, as shown in Fig. 1. Using 3D methods (Schuetz et al. 2010) 95 % of the backbone resonances could be sequentially assigned. The remaining resonances were assigned with 2D $^{13}C-^{13}C$ and 2D $^{13}C-^{15}N$ spectra and all but one resonance were assigned (99.6 %). The chemical shifts have been deposited in the BMRB under the accession number 19393. All residues of the peptide are visible in spectra based on dipolar transfers, indicating that they are all rigid. In particular, also the N-terminal part of Aβ that has been described as being flexible in wt-Aβ (Fändrich et al. 2011) yields strong, narrow resonances. A representative strip plot of the sequential assignment is shown in Fig. 2. For residues 11−14, 24−31 and 34, two or three sets of resonances are observed (vide infra). The intensity of the second set of resonances with respect to the main resonances varies for the different fibril preparations ([U−^{13}C,^{15}N], and [U−^{13}C]) studied between 60 and 10 %. We were able to reduce the amount of polymorphic fibrils in the [U−^{13}C] rotor to 10 % by removing the fibrils from the rotor, resuspending them in water and repacking the rotor. This, combined with the fact that the resonances are sharp (ca. 0.5 ppm linewidth) indicates that the fibril is well ordered and the packing of the monomers is highly symmetric. The second set of resonances must be from fibrils of a different morphology that have different sedimentation properties and cannot be due to structural inhomogeneity within the fibril. Figure 3a shows an overlay of DARR spectra of the two fibril preparations, the [U−^{13}C,^{15}N] sample 1 (in red), and the [U−^{13}C] (in blue)

sample 2 after washing. In the 1D extracts in Fig. 3b, it can be seen that the resonances in sample 2 are sharper, and the minor signals are greatly attenuated.

In Fig. 4, an extract of the aromatic region of a PAIN spectrum illustrates the disorder observed for the His14 side chain resonances, displaying the tentative assignment of the broad 14H Ne2 resonance clearly correlating to 14H Cγ. 14H Nδ1 is the only unassigned spin, since no signal could be observed for it. Figure 5 shows the assignment graph to illustrate the completeness of the assignments of the major polymorph.

The secondary chemical shifts (Fig. 6) and the secondary structure prediction with TALOS+ (Shen et al. 2009) are consistent with most of the protein being in β-sheet conformation. Clear exceptions are residues E 3 and G 25, which show chemical shifts corresponding to turns. Gly 9, Phe 20, Asp 23, Gly 33 and Gly 37 have non β-sheet chemical shifts but the TALOS+ prediction of the secondary structure is inconclusive. The secondary chemical shifts of the minor polymorph of His 14 is indicative of a turn, in contrast to the His 14 resonances of the major polymorph.

Figure 7 compares the secondary structure derived from the sequential assignments to values reported in the literature. As evidenced by the different location of the arrows for nearly all data shown, Aβ1−40 E22Δ shows a different conformation from all until now sequentially assigned forms of Aβ. The near-complete assignment of the major polymorph of Aβ1−40 E22Δ forms the basis for high-resolution 3D structure determination of this important Aβ variant.

Acknowledgments We would like to thank Andreas Hunkeler for technical support and Hiang Dreher-Teo for providing TEV protease. This work was supported by the Agence Nationale de la Recherche (ANR-12-BS08-0013-01), the ETH Zurich, the Swiss National Science Foundation (Grants 200020_124611, 200020_146757) and the NCCR program "Neural Plasticity and Repair" and the Centre National de la Recherche Scientifique. We also acknowledge support from the European Commission under the Seventh Framework Programme (FP7), contract Bio-NMR 261863.

References

Bertini I, Gonnelli L, Luchinat C, Mao J, Nesi A (2011) A new structural model of Aβ40 fibrils. J Am Chem Soc 133(40): 16013–16022

Böckmann A, Gardiennet C, Verel R, Hunkeler A, Loquet A, Pintacuda G, Emsley L, Meier BH, Lesage A (2009) Characterization of different water pools in solid-state NMR protein samples. J Biomol NMR 45(3):319–327

Castellani F, van Rossum B, Diehl A, Rehbein K, Oschkinat H (2003) Determination of solid-state NMR structures of proteins by means of three-dimensional N-15-C-13-C-13 dipolar correlation spectroscopy and chemical shift analysis. Biochemistry 42(39): 11476–11483

Debelouchina GT, Platt GW, Bayro MJ, Radford SE, Griffin RG (2010) Magic angle spinning NMR analysis of beta2-microglobulin amyloid fibrils in two distinct morphologies. J Am Chem Soc 132(30):10414–10423

Fändrich M, Schmidt M, Grigorieff N (2011) Recent progress in understanding Alzheimer's β-amyloid structures. Trends Biochem Sci:1–8

Franks W, Wylie B, Frericks Schmidt H, Nieuwkoop A, Mayrhofer R-M, Shah G, Graesser D, Rienstra CM (2008) Dipole tensor-based atomic-resolution structure determination of a nanocrystalline protein by solid-state NMR. Proc Natl Acad Sci 105: 4621–4625

Hardy J, Selkoe DJ (2002) The amyloid hypothesis of Alzheimer's disease: progress and problems on the road to therapeutics. Science 297(5580):353–356

Irie K, Murakami K, Masuda Y, Morimoto A, Ohigashi H, Ohashi R, Takegoshi K, Nagao M, Shimizu T, Shirasawa T (2005) Structure of beta-amyloid fibrils and its relevance to their neurotoxicity: implications for the pathogenesis of Alzheimer's disease. J Biosci Bioeng 99(5):437–447

Levy-Lahad E, Wasco W, Poorkaj P, Romano DM, Oshima J, Pettingell WH, Yu CE, Jondro PD, Schmidt SD, Wang K (1995) Candidate gene for the chromosome 1 familial Alzheimer's disease locus. Science 269(5226):973–977

Lopez del Amo J-M, Schmidt M, Fink U, Dasari M, Fändrich M, Reif B (2012) An asymmetric dimer as the basic subunit in Alzheimer's disease amyloid β fibrils. Angew Chem Int Ed 51(25):6136–6139

Loquet A, Bardiaux B, Gardiennet C, Blanchet C, Baldus M, Nilges M, Malliavin T, Böckmann A (2008) 3D Structure Determination of the Crh Protein from Highly Ambiguous Solid-State NMR Restraints. J Am Chem Soc 130(11):3579–3589

Manolikas T, Herrmann T, Meier BH (2008) Protein structure determination from 13C spin-diffusion solid-state NMR spectroscopy. J Am Chem Soc 130(12):3959–3966

Ovchinnikova OY, Finder VH, Vodopivec I, Nitsch RM, Glockshuber R (2011) The Osaka FAD mutation E22Δ leads to the formation of a previously unknown type of amyloid β fibrils and modulates Aβ neurotoxicity. J Mol Biol 408(4):780–791

Schuetz A, Wasmer C, Habenstein B, Verel R, Greenwald J, Riek R, Böckmann A, Meier BH (2010) Protocols for the sequential solid-state NMR spectroscopic assignment of a uniformly labeled 25 kDa protein: HET-s(1−227). ChemBioChem 11(11):1543–1551

Shen Y, Delaglio F, Cornilescu G, Bax A (2009) TALOS plus: a hybrid method for predicting protein backbone torsion angles from NMR chemical shifts. J Biomol NMR 44(4):213–223

Stevens TJ, Fogh RH, Boucher W, Higman VA, Eisenmenger F, Bardiaux B, van Rossum B-J, Oschkinat H, Laue ED (2011) A software framework for analysing solid-state MAS NMR data. J Biomol NMR 51(4):437–447

Tomiyama T, Nagata T, Shimada H, Teraoka R, Fukushima A, Kanemitsu H, Takuma H, Kuwano R, Imagawa M, Ataka S, Wada Y, Yoshioka E, Nishizaki T, Watanabe Y, Mori H (2008) A new amyloid beta variant favoring oligomerization in Alzheimer's-type dementia. Ann Neurol 63(3):377–387

Tycko R (2006) Molecular structure of amyloid fibrils: insights from solid-state NMR. Q Rev Biophys 39(1):1–55

Tycko R (2011) Solid-state NMR studies of amyloid fibril structure. Annu Rev Phys Chem 62(1):279–299

Van Melckebeke H, Wasmer C, Lange A, Ab E, Loquet A, Böckmann A, Meier BH (2010) Atomic-resolution three-dimensional structure of HET-s(218-289) amyloid fibrils by solid-state NMR spectroscopy. J Am Chem Soc 132(39):13765–13775

Vranken WF, Boucher W, Stevens TJ, Fogh RH, Pajon A, Llinas M, Ulrich EL, Markley JL, Ionides J, Laue ED (2005) The CCPN data model for NMR spectroscopy: development of a software pipeline. Proteins 59(4):687–696

Wang Y, Jardetzky O (2002) Probability-based protein secondary structure identification using combined NMR chemical-shift data. Protein Sci 11(4):852–861

Wasmer C, Lange A, van Melckebeke H, Siemer AB, Riek R, Meier BH (2008) Amyloid fibrils of the HET-s(218-289) prion form a beta solenoid with a triangular hydrophobic core. Science 319(5869):1523–1526

Wishart DS, Sykes BD (1994) The 13C chemical-shift index: a simple method for the identification of protein secondary structure using 13C chemical-shift data. J Biomol NMR 4(2):171–180

Zech SG, Wand AJ, McDermott AE (2005) Protein structure determination by high-resolution solid-state NMR spectroscopy: application to microcrystalline ubiquitin. J Am Chem Soc 127(24):8618–8626